JOURNAL OF GEOPHYSICAL RESEARCH, VOL. 99, NO. A4, PAGES 6079–6092, APRIL 1, 1994

# Imaging the effect of dipole tilt on magnetotail boundaries

C. Max Hammond,[1,2] Margaret G. Kivelson,[1] and Raymond J. Walker
Institute of Geophysics and Planetary Physics, University of California, Los Angeles

Eight years of IMP 8, four years of ISEE 2, and one year of IMP 7 magnetometer data have been combined to produce an "image" of the average magnetic field for a *YZ* cross section (aberrated GSM) of the magnetotail at a downtail distance of 25 $R_E$. The shape of the neutral sheet and magnetopause boundaries can be observed directly from the images. A fitting function that qualitatively matches the observed boundary shape can then be chosen. This approach improves on previous fits to possibly unsuitable functional forms specified independently of the data. In addition, as a refinement of previous studies, we have corrected for varying solar wind dynamic pressure and the effects of tail flaring. We find the magnetopause is displaced above the *XY* plane with increasing dipole tilt. The neutral sheet is found to curve slightly more than the model of Fairfield (1980) during times of large dipole tilt and near the flanks appears to differ substantially from the neutral sheet shape given by the analytic model of Voigt [1984], the more recent neutral sheet model of Dandouras (1988) based on the Voigt model, and the semi-empirical model of Tsyganenko (1989).

## INTRODUCTION

Most of the early studies of the neutral sheet [*Murayama*, 1966; *Bowling*, 1974; *Bowling and Russell*, 1976; *Russell and Brody* 1967] were exploratory in nature and made use of relatively small data sets. The circular arc model of the neutral sheet proposed by Russell and Brody was refined to an arc of an ellipse centered on the earth sun line by *Fairfield and Ness* [1970]. In general, these studies used the location of the change in sign of the *X* component of the field to identify the position of the neutral sheet.

Later, *Fairfield* [1980] used a larger data set consisting of several years of Imp 6, 7, and 8 data. Fairfield assumed a parametric equation to represent the neutral sheet shape and selected model parameters to minimize the number of data with the wrong $B_x$ polarity. Such a technique has the advantage of utilizing more information than studies which simply fit locations of changes in sign of the *X* component of the field. For example, one can imagine in a poorly sampled region an individual neutral sheet crossing, identified by the switch in polarity with no weighting by the time the spacecraft was in the spatial region of the type peformed by *Dandouras* [1988], occurring at a place where on average the field polarity was consistent with being above the neutral sheet. Whereas fits to neutral sheet crossings would be shifted by such an observation, the technique of Fairfield would be unaffected as most of the sampled points would still have the correct polarity. The technique of Dandouras would also not be affected since such points would receive very little weighting in the fit.

Fairfield also introduced the idea that the neutral sheet could be represented as a displaced ellipse which can be placed so that the two lobes have equal areas and thus equal magnetic flux assuming that the magnitude of the field is, on average, identical in the two lobes (an assumption supported by the present work). However, as noted by Gosling et al. [1986], while Fairfield introduced this idea of a displaced ellipse, the neutral sheet model determined by Fairfield does not maintain equal lobe areas during times of extreme dipole tilt angle assuming a cylindrical magnetopause centered on the earth-sun line. One drawback of the Fairfield technique is that the functional form of the neutral sheet is specified before the optimization of the fit is done. In addition, if data used in the study of Fairfield are sampled uniformly in time, then the resultant fit will be optimized for a dipole tilt of approximately 12°, the dipole tilt at which the Earth spends the majority of its time during a given year. Fairfield also did not correct for the expansion of the tail with decrease of solar wind pressure nor did he account for changes in the apparent location of the neutral sheet due to tail flaring.

More recently, *Dandouras* [1988] studied the neutral sheet position using ISEE 1 data. He fit a boundary formed by the intersection of three ellipses to locations where the $B_x$ component changed sign and he weighted the data by the time the spacecraft was in a spatial bin. During times of large dipole tilt angle this model differs significantly from the model of Fairfield especially on the flanks. However, the Dandouras model is based on data taken closer to the Earth than that of Fairfield which may account for some of this difference. As in the Fairfield work, no correction was made for either the expansion of the tail cross section with decrease in solar wind pressure or the effects of tail flaring.

Previous observational studies of the shape of the magnetopause boundary have concentrated on the dayside or have assumed axial symmetry and determined the radial variation of the magnetopause with downtail distance. Recently *Ohtani and Kokubun* [1990] have suggested that the magnetopause is flattened in the north south direction. Ohtani and Kokubun, however, ignored dipole tilt effects. Simulations by *Walker et al.* [1989] suggest that the cross-sectional boundary of the magnetopause distorts from a circular, axially symmetric shape during times of large dipole tilt, becoming slightly egg shaped while still maintaining equal areas in the

[1]Also at Department of Earth and Space Sciences, University of California, Los Angeles.

[2]Now at Los Alamos National Laboratory, Los Alamos, New Mexico.



Paper number 93JA01924.
0148-0227/94/93JA-01924$05.00

lobes. In the Walker et al. simulation the east west extent is greater in the northern lobe than in the southern lobe during positive dipole tilts giving rise to the egg shape. This suggests the assumption of full north-south symmetry of the boundary shape may be invalid for large dipole tilt angles.

## DATA

In this paper we form images of the average magnetic structure in a 60×60 $R_E$ plane perpendicular to the aberrated earth-sun line. Figure 1 shows a schematic summary of the data processing. The processing obtains median values of the vector magnetic field in 0.6 $R_E$ square bins for a $YZ_{AGSM}$ (aberrated GSM) cross section of the magnetotail. The data in this study are 60-s resolution magnetometer data from the IMP 8 spacecraft during the time span 1978-1986 and the ISEE 2 spacecraft for the years 1978, 1979, 1984, and 1986. In addition, one year (1973) of IMP 7 magnetometer data was used. IMP 8 and IMP 7 had nearly circular orbits between 30 and 40 $R_E$ in radius while ISEE 2 had an elliptical orbit with an apogee of ~23 $R_E$. All field values and coordinates were rotated to aberrated GSM coordinates by using an aberration angle of 4°. The aberrated GSM (AGSM) coordinate system is defined with $X$ along the aberrated solar wind flow direction; the $XZ$ plane contains the dipole axis, and $Y$ completes the right-handed coordinate system.

One can expect the solar wind dynamic pressure to control the scale size of the magnetotail and, correspondingly, the location of the magnetopause boundary in the tail. We used the OMNI solar wind data set (obtained from the National Space Science Data Center) consisting of hourly averages of solar wind parameters to apply a simple one sixth power scaling to the spatial coordinates based on the ratio of the solar wind dynamic pressure to a reference solar wind dynamic pressure of $3.8\times10^{-9}$ Pa. On the dayside, the magnetopause appears to be less affected by solar wind dynamic pressure during times of southward interplanetary magnetic field (IMF) than during periods of northward IMF [*Sibeck et al.*, 1991; *Petrinec et al.*, 1991]. However a significant effect of solar wind dynamic pressure still remains regardless of the IMF direction and in the present work we have neglected any $B_z$ effect when scaling by dynamic pressure.

Recently, *Russell and Petrinec* [1992] have shown that when used as solar wind monitors, different particle instruments on the same spacecraft or two different spacecraft may differ significantly in their measurement of solar wind density. The study of Russell and Petrinec used the original

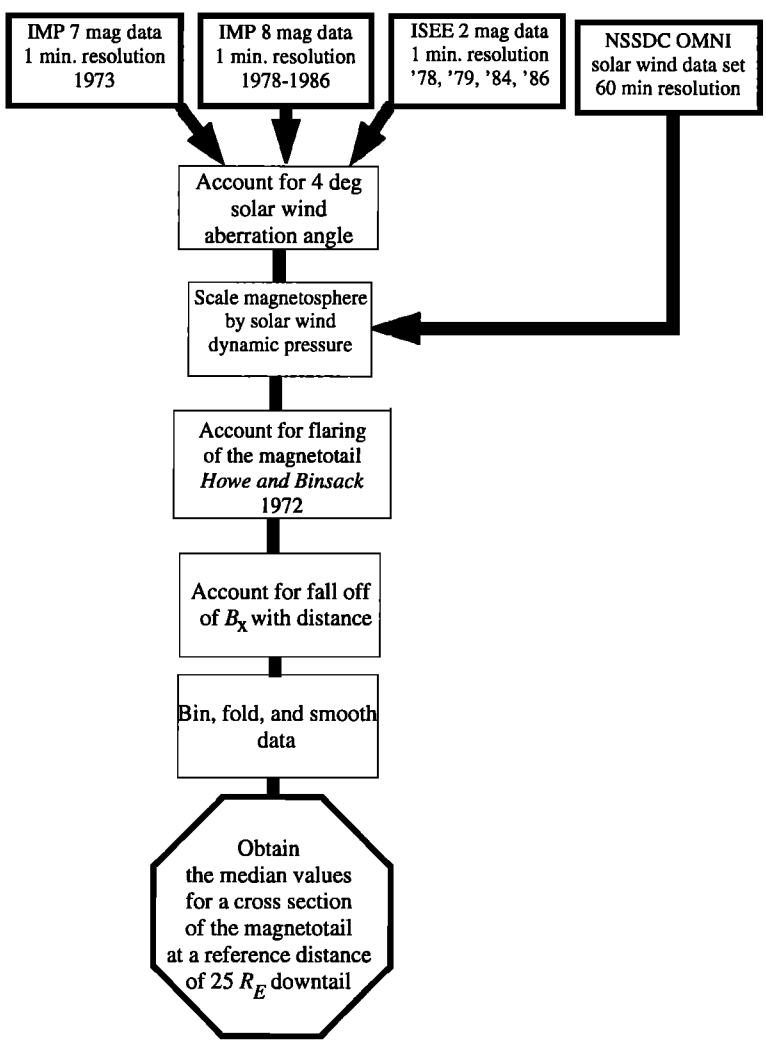


Fig. 1. Schematic representation of the data processing.

solar wind data submitted to the NSSDC rather than the OMNI data set. The densities from differing instruments and spacecraft have been cross normalized in the OMNI data set [*Couzens and King*, 1985]. The dynamic pressures used in this study are only as accurate as the calibrations and timings used in the OMNI data set allow.

Because the tail flares, the cross section at fixed solar wind dynamic pressure varies with downtail distance. In order to obtain a cross-sectional image of the magnetotail representative of a single downtail distance, both the magnetic field values and coordinates were rescaled to represent the cross section at $X_{AGSM}$=-25 $R_E$. The flaring magnetopause model of *Howe and Binsack* [1972] was used in the coordinate scaling. The Howe and Binsack model gives the tail radius solely as a function of downtail distance with no dependence on activity or solar wind parameters. A recent study has shown that the flaring angle also depends on both the dynamic pressure and on magnetic activity as characterized by the *AL* index [*Nakai et al.*, 1991]. However, a similar study to that of Nakai et al. reports that downtail distance is the dominant factor in determining tail size [*Ohtani and Kokubun*, 1990]. Consequently, we have not corrected the tail flaring angle for either dynamic pressure or activity. In addition, we have minimized the effect of errors in scaling by choosing a reference distance of 25 $R_E$ down the tail. Because the data were restricted to downtail distances -15 $R_E \geq X_{AGSM}$ > -35 $R_E$, no value to be scaled was greater than 10 $R_E$ from the reference position. The restriction of downtail distances to the range -15 $R_E \geq X_{AGSM}$ > -35 $R_E$ also avoids the transition region in which the neutral sheet joins the magnetic equator [*Peredo and Stern*, 1991].

The magnetic field values were scaled with distance using

$$B \propto |X_{AGSM}|^{-0.0365Kp-0.543} \qquad (1)$$

The coefficients in (1) were determined by using a subset of the data restricted to time intervals when the dipole tilt was <5° by a nonlinear optimization technique. The data used in the generation of (1) were restricted to locations where the radial distance of the spacecraft from the $X_{AGSM}$ axis was approximately between 10 and 17.5 $R_E$ and the angle of this radius vector in the $YZ_{AGSM}$ plane was between 30° and 150° or -30° and -150° where the angle is measured from the *Y* axis. This geometrical restriction alone does not guarantee that all selected intervals are in the lobes. However, as will be seen when we discuss Plate 1 the nominal lobe location as identified by this restriction corresponds to spatial bins with a low standard deviation of the field. Undoubtedly, some plasma sheet field measurements are included in the data set. However, (1) does not differ greatly from other expressions for the field fall off with distance. Thus we believe that the choice of (1) instead of another of the expressions plotted in Figure 2 has little effect on our results. Figure 2 shows the lobe field versus *X* during times of low and high activity for the *Behannon* [1968], *Mihalov et al.* [1968], and *Nakai et al.* [1991] models, and for the present model given by (1). For the Nakai et al. model we have used average values of the solar wind dynamic and magnetic pressure and β in the solar wind was assumed to be 2. For the present model in Figure 2 , *Kp* values of 1 and 5 were used for the low- and high-activity cases respectively. The Mihalov et al. model was based on *Kp* values ≤2+ and thus is not shown on the high *Kp* case in Figure 2. The Behannon model also tends to underestimate the field in the high *Kp* case.

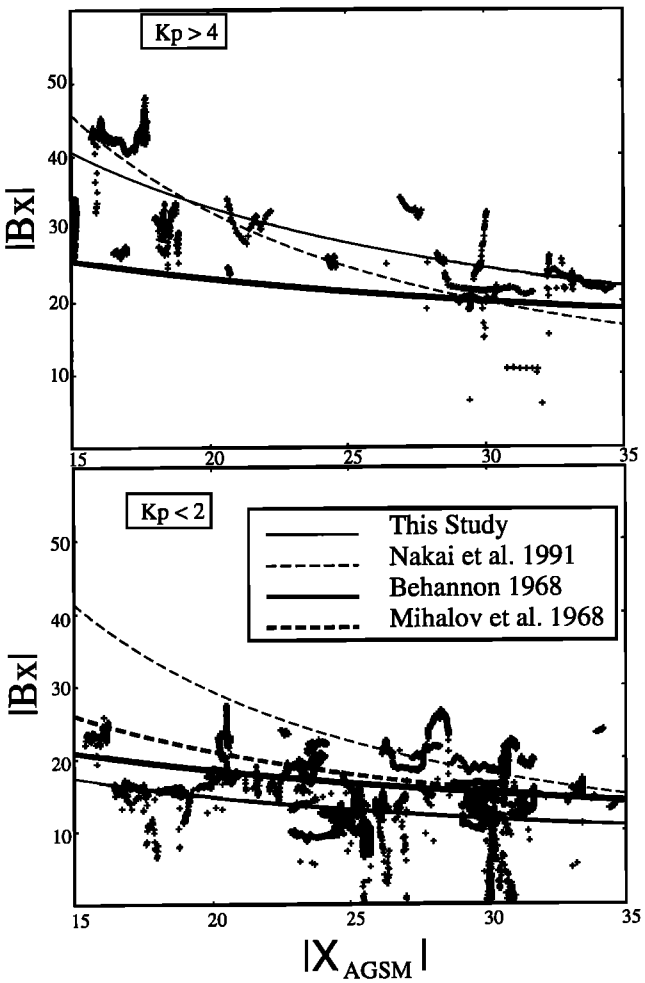


Fig. 2. The value of $|B_x|$ versus downtail distance for *a)* $Kp \leq 2$ *b)* $Kp \geq 4$. The solid line is the model presented in this study by using *Kp* of 1 and 5 for the low and high activity cases respectively. The dashed line is from the model of *Nakai et al.* [1991] using average values for the solar wind pressures and an *AL* of 25 and 400 for the low and high activity cases respectively. The heavy solid line is from *Behannon* [1968] using *Kp* of 1 and 5 for the low- and high-activity cases respectively. The heavy dashed line is from *Mihalov et al.* [1968]. Note the Mihalov et al. fit was based on data in which $Kp \leq 2^+$ and so is not shown for the $Kp \geq 4$ case.

*Nakai et al.* [1991] have also reported a fit to the variation of *B* with distance in the tail. They proposed

$$B = \left(\frac{R}{20}\right)^{-1.2} \left(aP_D + bP_S + c|AL| + d\right)$$

where

$$a = 1.94 \times 10^8 \qquad (2)$$
$$b = 7.78 \times 10^9$$
$$b = 8.28 \times 10^{-3}$$
$$d = 19.6$$

*R* is the geocentric distance. $P_D$ and $P_S$ are the dynamic and static solar wind pressure in dynes/cm$^2$, *AL* is the geomagnetic index, and *d* is measured in nanoteslas.

The recent work by *Nakai et al.* [1991] fits the field magnitude in the tail to a form that not only decreases with distance down the tail (with an exponent of -1.2) but also increases with both activity and solar wind dynamic pressure and static pressure. The fit given in (1) and plotted in Figure 2

does not include the effect of solar wind pressure. Nonetheless, the goodness of fit to the data of this study, as quantified by $\chi^2$, is better for the fits from (1) ($\chi^2$ values of 26 and 40 for the low- and high-$Kp$ ranges, respectively), than for the fits to the Nakai et al. expression ($\chi^2$ values of 96 and 59 for the low- and high-$Kp$ ranges, respectively). It is likely that had the instantaneous solar wind dynamic pressure rather than the nominal value been used in the evaluation of $\chi^2$ for the Nakai et al. model the value of $\chi^2$ would have been lower. By adopting (1) the effect of dynamic pressure on field magnitude remains in our data set. In fact, our approach to scaling the dimensions of the magnetosphere by increasing all linear dimensions (including $X$) as the solar wind dynamic pressure increases amplifies the dependence of the field magnitude on the solar wind pressure. By assigning a measured field value to an $X$ value that moves tailward as the solar wind dynamic pressure rises, one causes the field magnitude at a fixed reference distance to vary proportionally with solar wind dynamic pressure. The effect, then, of solar wind dynamic pressure on field magnitude remains in our dataset and is slightly amplified by our scaling of the spatial coordinates by dynamic pressure. However, the results are quite insensitive to this feature of the data treatment for two reasons. First, the reference distance is taken at $X_{AGSM}$=-25 $R_E$, in the middle of the -15 to -35 $R_E$ range measured. Second, the average solar wind dynamic pressure is close to the same (~3 nPa) for each of the dipole tilt bins that are used, as shown in Figure 3. As the objective of the study is to determine the effect of dipole tilt on the boundaries, the failure to correct properly for solar wind dynamic pressure variations introduces scatter in the results but does not change them.

After scaling both the position and field values to represent a cross section at $X_{AGSM}$=-25 $R_E$, the data were binned into 0.6 by 0.6 $R_E$ bins extending from $-30 \le Y_{AGSM} \le 30$ $R_E$ and $-30 \le Z_{AGSM} \le 30$ $R_E$. This 60×60 $R_E$ box safely encompasses the nominal magnetopause width of 46.7 $R_E$ appropriate for a downtail distance of 25 $R_E$ as determined from the model of *Howe and Binsack* [1972].

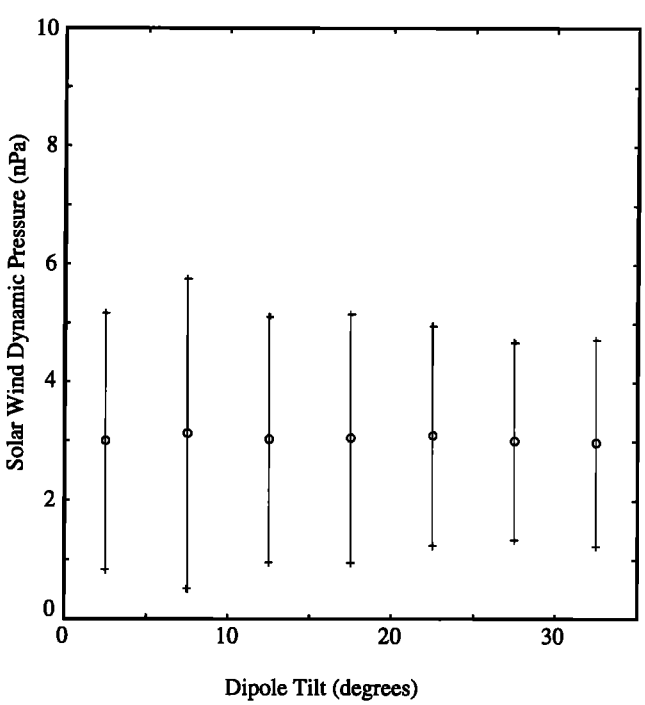


Fig. 3. Average solar wind dynamic pressure in nanopascals for 5° dipole tilt bins. Crosses show the locations of ±1 standard deviation.

In the images that follow, the data have been both folded and smoothed. We have assumed that the tail is symmetric across the $Z_{AGSM}$ axis and folded the data across this axis. A seasonal folding has also been introduced. For data acquired during times of negative dipole tilt, the signs of both the $Z_{AGSM}$ coordinate and the $X$ and $Y$ components of the field have been changed. Our results are thus presented as if all the data were taken during northern hemisphere summer. The data were smoothed by linking data in a bin to data in all eight adjacent bins. Bins were rejected as having too few data points to be statistically significant if the linked bins contained fewer than 10 1-min data points.

One expects the magnetosheath field to be highly variable with no preferential direction in contrast to the steady $\pm X$ directed lobe field. Using this difference between characteristic lobe and sheath magnetic fields, possible magnetosheath bins were taken to be those in which $\sigma_n$, defined as the sum of the standard deviations of the three components of the field normalized by the average $X$ component of the field in the bin, was $\ge 1.5$. Plate 1 shows the value of $\sigma_n$ for all cross sectional bins. As is evident from Plate 1, there are several distinct regions of high and low variation of the field. The lack of a gradual change between the two regions around a nearly circular boundary justifies the use of this parameter as an indicator of the average location of the magnetopause. We will see later that the magnetopause radius found in this manner agrees well with the predicted value for the magnetopause radius from the model of *Sibeck et al.* [1991]. Plate 1 also shows that the central plasma sheet boundaries across the center of the tail may be identified from this parameter.

Inspection of the boundaries evident in the images of the magnetotail suggest a form for a model that provides a relevant expression for the boundaries. A rigorous determination of the boundary locations is needed to determine the parameters of the model. The magnetopause boundary was determined by finding the sheath-lobe interface along radial spokes starting 1 $R_E$ outward from the nominal magnetopause position of Howe and Binsack and stepping inward to 8 $R_E$ from the starting point. The sheath lobe interface was defined as the boundary between 0.6×0.6 $R_E$ bins with $\sigma_n \ge 1.5$ (magnetosheath) and $\sigma_n < 1.5$ (lobe) as discussed above. Along some radial spokes there are bins that contain no data. No interface was recorded for a particular spoke if, in moving inward along the radial spoke, consecutive empty bins span more than 1.5 $R_E$ between sheath and lobe bins or if no sheath bins are found within 8 $R_E$ from the starting point. Bins in which $\sigma_n \ge 1.5$ but all 8 adjacent bins had $\sigma_n < 1.5$ were ignored. The procedure was repeated every 2° around the $X_{AGSM}$ axis. No sheath-lobe interface determination was made if the distance along $Z_{AGSM}$ from the model neutral sheet was within ±4 $R_E$ to avoid the region where the criterion on $\sigma_n$ fails to distinguish between plasma sheet and magnetosheath. Along a radial spoke there can be multiple bins in which the interface selection criteria is met. Because there is no reason to prefer one interface over the next all instances of an interface along a radial spoke were recorded.

The neutral sheet was determined by starting from -9 $R_E$ (-3 $R_E$ for the small dipole tilt angle case) below the $Z$=0 plane and moving along $Z$ until the bin was found at which the median value of the field changes sign. This was done for $Y$ values between ±22 $R_E$. The locations of both the neutral sheet and magnetopause boundary points are shown in Figure 4 for 5°

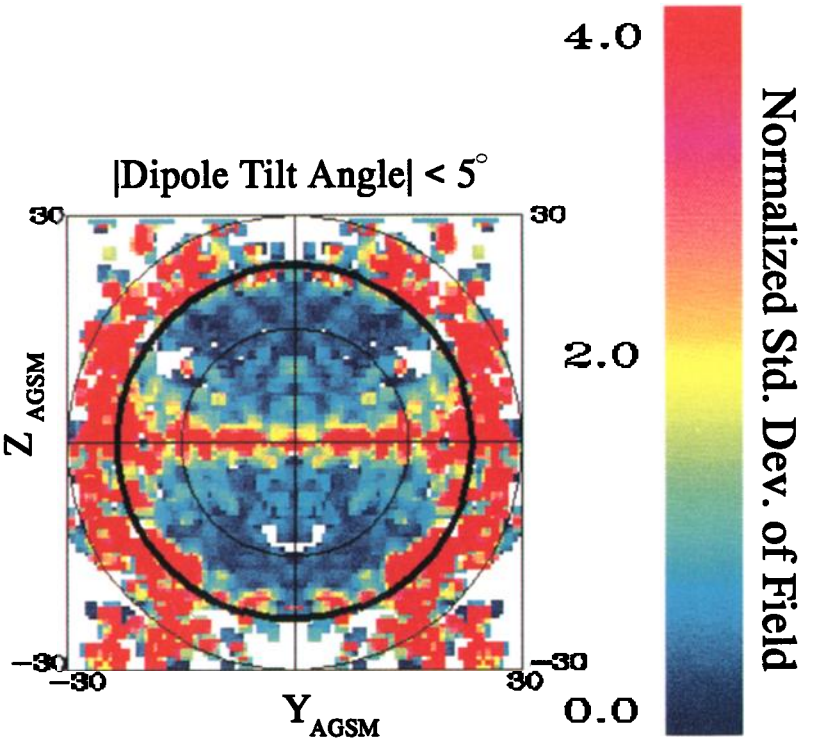


Plate 1. Normalized standard deviation, $(\sigma_x + \sigma_y + \sigma_z)/\langle B_x \rangle$, in each bin represented by the color scale for a 60 × 60 $R_E$ cross-sectional slice of the magnetotail at $X_{AGSM}$=-25 $R_E$ for a nominal solar wind dynamic pressure of 3.8 nPa during times when the absolute value of the dipole tilt angle was < 5°. Thin circles denote radial distances from the $X_{AGSM}$ axis of 15 and 30 $R_E$. The heavy black line is the model magnetopause of *Howe and Binsack* [1972].

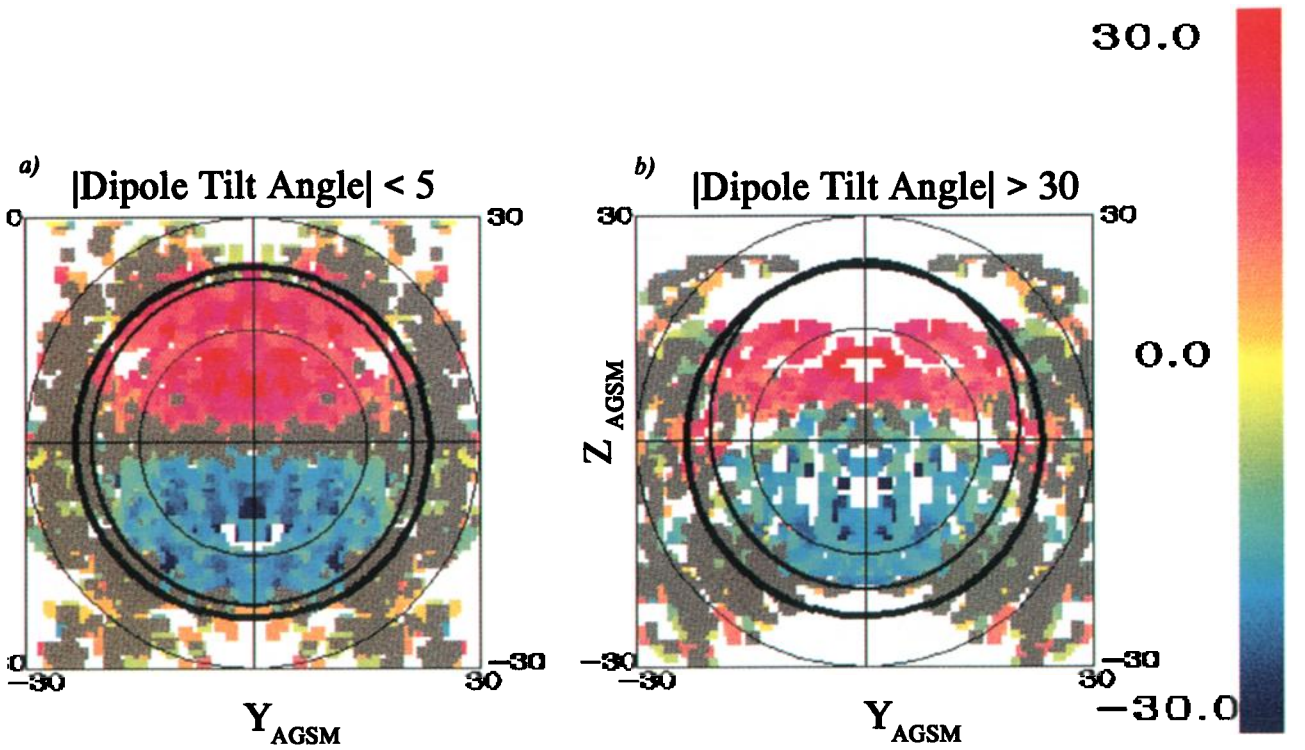


Plate 2. Median value of $Bx_{AGSM}$ in 0.6×0.6 $R_E$ bins for a 60 × 60 $R_E$ cross section of the magnetotail at $X_{AGSM}$=-25 $R_E$ for a nominal solar wind dynamic pressure of 3.8 nPa during times when the dipole tilt angle was *(a)* < 5° and *(b)* ≥ 30°. The color scale gives the values in nanoteslas. Gray represents the magnetosheath and the plasma sheet as explained in the text. The heavy black line is the model magnetopause of *Howe and Binsack* [1972]. The thin black line is the model magnetopause for the two dipole tilt extremes presented in this study. The very thin lines are grid lines denoting radial distances from the $X_{AGSM}$ axis of 15 and 30 $R_E$.

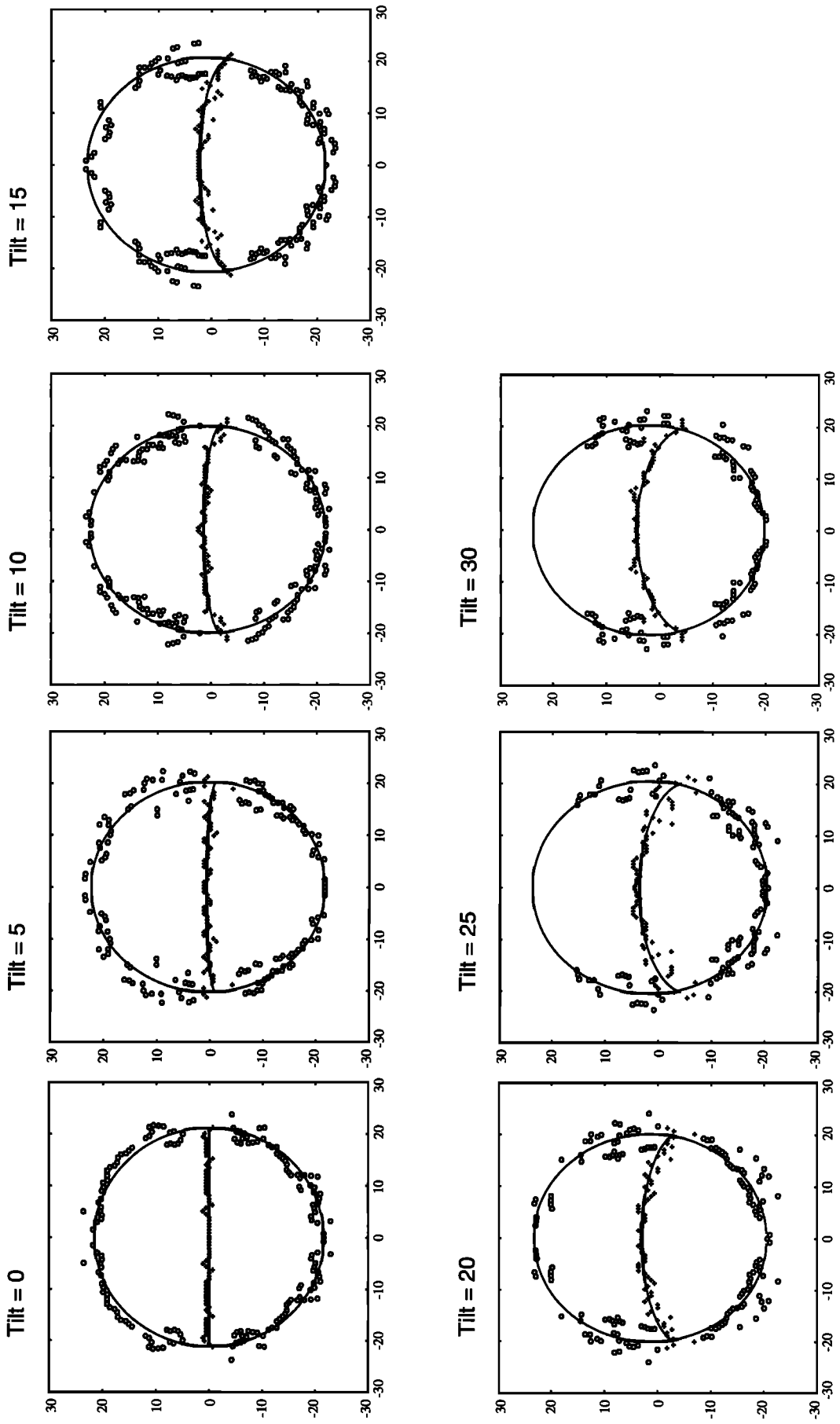


Fig. 4. Magnetopause (open circles) and neutral sheet (crosses) boundaries for 5° intervals of dipole tilt angle. The solid lines are the best fits to these points as discussed in the text.

increments of dipole tilt. Also shown are the model fits to these points discussed below.

## RESULTS

Plate 2 shows a 60×60 $R_E$ slice in the $YZ_{AGSM}$ plane of the magnetotail during times when the absolute value of the dipole tilt was < 5° (Plate 2*a*) and during times when the absolute value of the dipole tilt was ≥ 30° (Plate 2*b*). Gray represents the magnetosheath and the central plasma sheet identified from $\sigma_n$ values as discussed above. White indicates bins for which fewer than 10 data points were available in the linked set of associated bins. The sign and magnitude of the $X$ component of the field are indicated by the color scale. The narrow dark curves represent the model fits to be described. The heavy dark line is the predicted magnetopause for a downtail distance of -25 $R_E$ from the magnetopause model of *Howe and Binsack* [1972]. The magnetopause in the data of Plate 2*b* appears distorted from its almost circular shape in Plate 2*a*. During times of large dipole tilt the magnetopause boundary appears to have contracted inward along the southern lobe. This is why we used a nonlinear optimization technique to fit the magnetopause boundary with a curve of the form:

$$Y=\beta\sqrt{1-\left(\frac{Z-\delta}{\alpha}\right)^2} \qquad (3)$$

where $Y$ and $Z$ are in AGSM coordinates and $\alpha$, $\beta$, and $\delta$ were determined from the data. As a constraint to the fit we imposed the condition of equal areas for the two lobes. The resulting parameters for 5° dipole tilt bins are shown in Table 1. The thin black curves in Figure 4 and Plate 2 are our fits to the data.

TABLE 1. Parameters of Model Magnetopause for 5° Increments of Y, the Dipole Tilt, Appropriate for a Downtail Distance of 25 $R_E$ and a Solar Wind Dynamic Pressure of 3.8 nPa

| Dipole Tilt Range | $a$ ($R_E$) | $b$ ($R_E$) | $d$ ($R_E$) |
|---|---|---|---|
| \|Y\| < 5° | 21.6 | 21.2 | 0.00 |
| 5° ≤ \|Y\| < 10° | 22.0 | 20.3 | 0.40 |
| 10° ≤ \|Y\| < 15° | 22.2 | 20.0 | 0.67 |
| 15° ≤ \|Y\| < 20° | 22.4 | 20.7 | 0.92 |
| 20° ≤ \|Y\| < 25° | 21.9 | 20.1 | 1.41 |
| 25° ≤ \|Y\| < 30° | 22.1 | 20.5 | 1.69 |
| \|Y\| > 30° | 21.8 | 20.3 | 2.11 |

Figure 5 shows the magnetopause parameters determined from the fits versus dipole tilt angle. During times of small dipole tilt angle, the magnetopause boundary is approximately circular with an average radius of 21.4 $R_E$ which agrees reasonably well with the 23.4 $R_E$ radius of the Howe and Binsack model. The value is in even better agreement with the 22.9 $R_E$ predicted by the *Sibeck et al.* [1991] magnetopause model for solar wind dynamic pressures between 2.6 and 4.9 nPa. On average, however, the magnetopause is slightly elliptical in shape with the north south axis approximately 22.0 $R_E$ while the east west axis is 20.4 $R_E$. In addition the whole magnetopause is displaced along the north-south axis. Figure 5 shows the displacement of the ellipse fitted to the sine of twice the dipole tilt angle. The factor of 2 accounts for the expected return to the origin for a 90° tilt. This implies that the maximum displacement would occur at 45°. This displacement of the magnetopause toward $Z_{AGSM}$ as the dipole tilt increases accounts for the contraction of the magnetopause boundary in the southern lobe seen in Plate 2. The parameters for (3) were determined to be

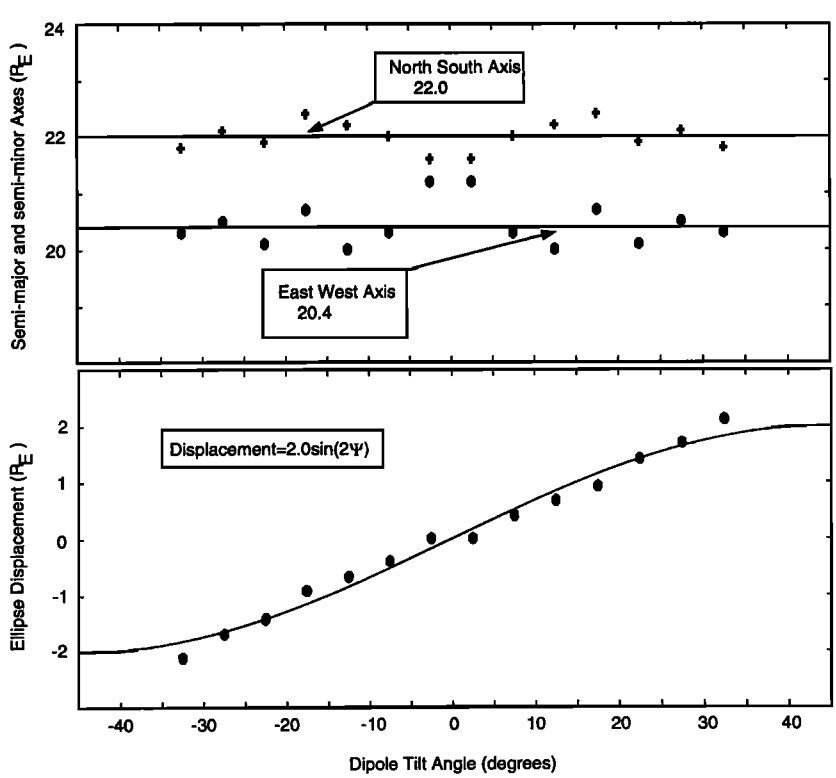


Fig. 5. Magnetopause parameters determined for each of the 5° dipole tilt bins from the magnetopause model given by (3). The top panel shows $\alpha$ (crosses), the north-south width of the magnetopause ellipse, and $\beta$ (filled circles), the east-west width of the magnetopause. The bottom panel shows the displacement of the magnetopause ellipse. Also shown are the modelled expressions for the variation of each parameter with dipole tilt.

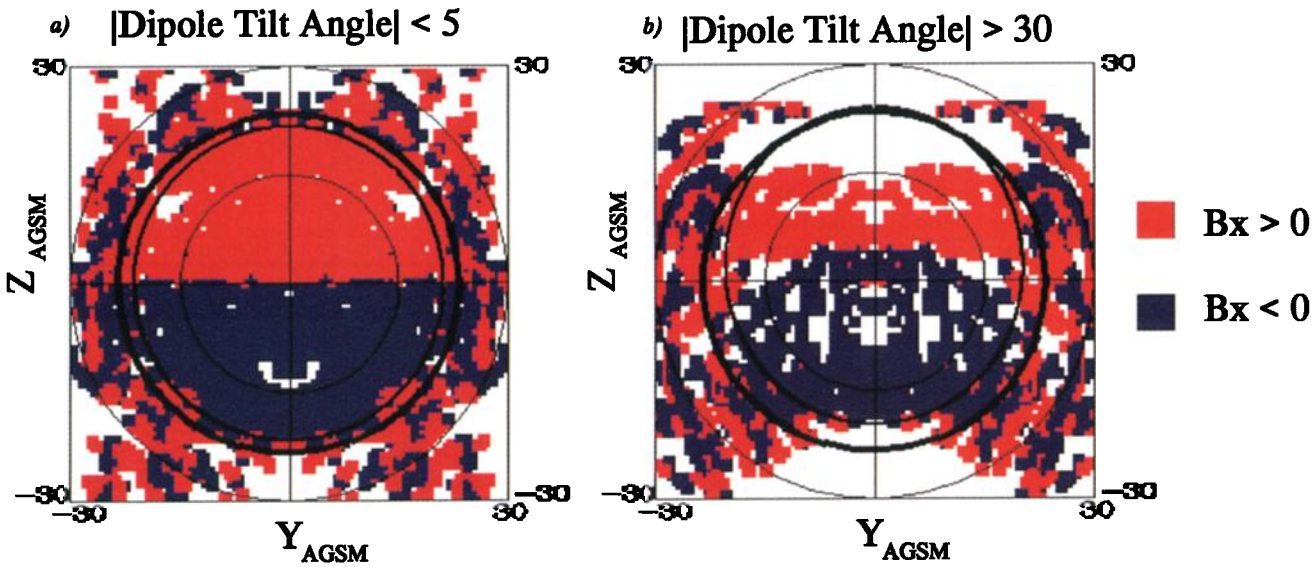


Plate 3. Plot of a $60 \times 60\ R_E$ cross section of the magnetotail similar to Plate 2. Red (blue) indicates positive (negative) values of the median value of $Bx_{AGSM}$ in each bin. *(a)* dipole tilt angle < 5°. *(b)* dipole tilt angle ≥ 30°.

$$\alpha = 22.0$$
$$\beta = 20.4 \qquad (4)$$
$$\delta = 2.0\sin(2\Psi)$$

where $\Psi$ is the dipole tilt angle. The exact values for $\alpha$ and $\beta$ depend on the value adopted for identifying the lobe bins. As is clear from Plate 1 the differences in absolute values for $\alpha$ and $\beta$ caused by choosing a higher value of $\sigma_n$ would be smaller than $2\ R_E$.

Plate 3 shows the same cross sectional slice of the magnetotail for the same two extremes of dipole tilt as in Plate 2 but here the sheath is not represented by gray; instead the model magnetopauses of Howe and Binsack and the present study are drawn. Red and blue represent positive and negative values of the $X$ component of the field. Viewed in this manner, the neutral sheet becomes prominent as the boundary between red and blue inside the nominal magnetopause boundary. As expected, during times of small dipole tilt the neutral sheet is a straight line (Plate 3*a*). During times of large dipole tilt the neutral sheet becomes curved (Plate 3*b*). Note that this curved neutral sheet appears elliptical supporting the *Fairfield* [1980] choice of an ellipse as the appropriate fitting curve. The model used by Fairfield is given by

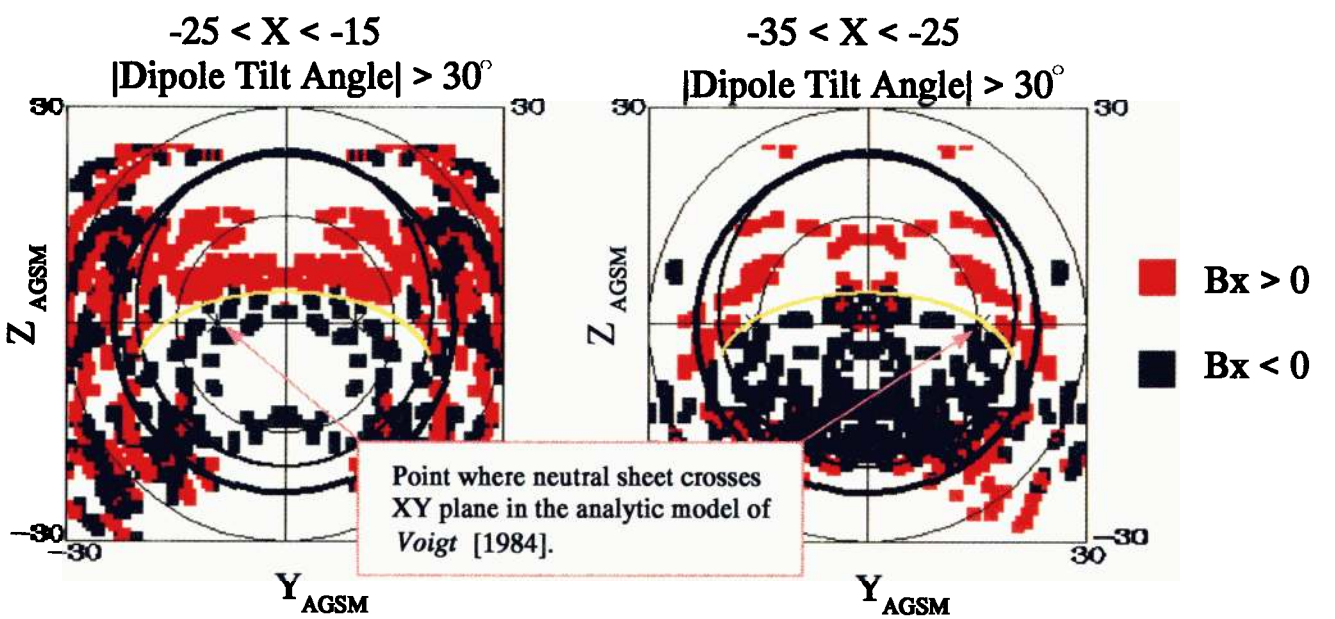


Plate 4. A plot of $60 \times 60\ R_E$ cross sections of the magnetotail for a nominal solar wind dynamic pressure of 3.8 nPa during times when the dipole tilt angle was ≥ 30° for downtail distances of $-15 \geq X_{AGSM} > -25$ and $-25 \geq X_{AGSM} > -35$. Asterisks mark the point where the scaled Voigt neutral sheet of Figure 7 crosses the $XY$ plane. The heavy dark line is the model magnetopause of *Howe and Binsack* [1972]. The thin black line is the model magnetopause from the present study. The very thin lines are grid lines denoting radial distances from the $X_{AGSM}$ axis of 15 and 30 $R_E$. The yellow line is the model neutral sheet from the present study.

TABLE 2. Parameters of Model Neutral Sheet From *Fairfield* [1980] and the Present Study which is Appropriate for a Downtail Distance of 25 $R_E$ and a Solar Wind Dynamic Pressure of 3.8 nPa

| Parameter | *Fairfield* [1980] | This Study |
|---|---|---|
| $H_0$ | 10.5 $R_E$ | 8.6 $R_E$ |
| $Y_0$ | 22.5 $R_E$ | 20.2 $R_E$ |
| $D$ | 14.0 $R_E$ | 12.2 $R_E$ |

$$Z_{NS} = \left[ (H_0 + D)\sqrt{\left(1 - \frac{Y^2}{Y_0^2}\right)} - D \right] \sin\Psi \quad |Y| < Y_0$$
$$Z_{NS} = -D\sin\Psi \quad |Y| \geq Y_0 \tag{5}$$

$Z_{NS}$ is the displacement of the neutral sheet above or below the $XY_{AGSM}$ plane. $H_0$ and $Y_0$ determine the ellipticity of the neutral sheet with $H_0 sin\Psi$ giving the displacement of the neutral sheet above the $XY_{AGSM}$ plane at the midnight meridian. $Dsin\Psi$ is the displacement of the ellipse below the $XY_{AGSM}$ plane, and $\Psi$ is the dipole tilt angle. Table 2 gives the result of our fit along with those parameters determined by Fairfield. Figure 4 shows this model and the data for each of the 5° dipole tilt bins.

The parameters given in Tables 1 and 2 are derived from data which has been scaled to account for dynamic pressure effects on the relative location of the observations and downtail distance effects. The complete equation for the magnetopause which includes these scalings is given by

$$Y = \beta'\sqrt{1 - \left(\frac{Z - \delta'}{\alpha'}\right)^2}$$
$$\alpha' = 22.0\left(\frac{3.8}{P_{obs}}\right)^{1/6} \theta(X_{AGSM})$$
$$\beta' = 20.4\left(\frac{3.8}{P_{obs}}\right)^{1/6} \theta(X_{AGSM}) \tag{6}$$
$$\delta' = 2.0\left(\frac{3.8}{P_{obs}}\right)^{1/6} \sin(2\Psi)$$

where $P_{obs}$ is the observed dynamic pressure in nano-Pascals. The dimensionless term $\theta(X_{AGSM})$ corrects for the changing tail radius by using the model magnetopause of *Howe and Binsack* [1972] and is given by

$$\theta(X_{AGSM}) = 1.02 \arctan\left(\sqrt{\frac{10 - X_{AGSM}}{15.9}}\right) \tag{7}$$

The corrections to the neutral sheet parameters are similar:

$$Z_{NS} = \left[ (H_0' + D')\sqrt{\left(1 - \frac{Y^2}{Y_0^2}\right)} - D' \right] \sin\Psi \quad |Y| < Y_0'$$
$$Z_{NS} = -D'\sin\Psi \quad |Y| \geq Y_0'$$
$$H_0' = 8.6\left(\frac{3.8}{P_{obs}}\right)^{1/6}$$
$$Y_0' = 20.2\left(\frac{3.8}{P_{obs}}\right)^{1/6} \theta(X_{AGSM}) \tag{8}$$
$$D' = 12.2\left(\frac{3.8}{P_{obs}}\right)^{1/6}$$

## DISCUSSION

Figure 6 shows several proposed neutral sheet models along with the neutral sheet model determined from this study. As evident from Figure 6 the neutral sheet model of *Fairfield* [1980] gives the approximate shape of the neutral sheet during times of large dipole tilt angle. The neutral sheet model presented here is basically a refinement of the Fairfield model. Part of this difference may be accounted for in the effect of solar wind dynamic pressure. The nominal solar wind pressure chosen to scale the spatial coordinates for the present study was $3.8\times10^{-9}$ Pa while Figure 3 shows that the actual observed average solar wind dynamic pressure was $3.0\times10^{-9}$ Pa. Thus the values from the present study shown in Tables 1 and 2 should be scaled by the ratio $(3.8/3.0)^{1/6}$ to account for the difference in the observed solar wind dynamic pressure during the time the parameters of the present study were determined and the arbitrarily chosen nominal solar wind dynamic pressure. Even after such scaling, however, the difference in the values of the parameters of this study and that of *Fairfield* [1980] are significant.

Figure 6 shows that the four models differ most near the flanks of the magnetotail where the present model neutral sheet differs significantly from the models of *Dandouras* [1988] and *Gosling et al.* [1986]. It should be noted, however, that the Dandouras and Gosling et al. models are based on ISEE data taken nearer to the earth than most of the data used here. Some difference in the neutral sheet models is due to the effects of tail flaring. There remains a difference in the basic shape of the Dandouras and Fairfield neutral sheets. *Dandouras* [1988] has pointed out the sampling bias which contributes to the large curvature of the Gosling et al. model sheet. The smaller difference in the present neutral sheet model and that of Dandouras is caused in large part because Dandouras chose a functional form that closely matches the neutral sheet shape from the analytic magnetospheric magnetic field model of *Voigt* [1984]. As can be seen in Figure 6 the Dandouras neutral

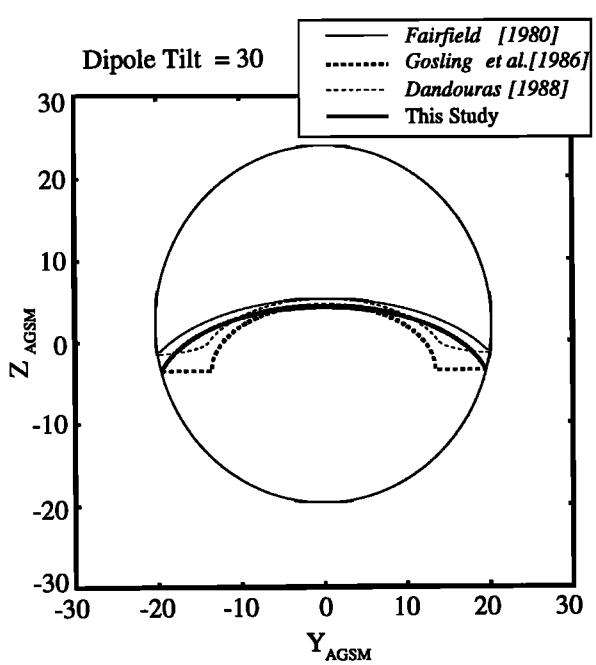


Fig. 6. Several previous model neutral sheets and the neutral sheet determined from this study all evaluated by using a dipole tilt of 30°. The neutral sheet shown for the present study is appropriate for a solar wind dynamic pressure of 3.8 nPa.

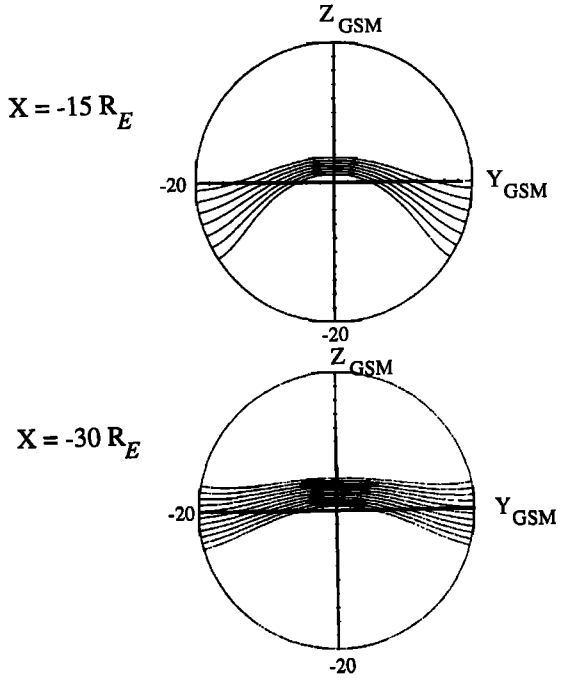


Fig. 7. Current streamlines for a 20 $R_E$ magnetopause for downtail distances of $X$=-15 $R_E$ and $X$=-30 $R_E$ . The middle streamline represents the neutral sheet. Adapted from Figure 4 of *Voigt* [1984].

sheet becomes roughly parallel to the $XY_{AGSM}$ plane near the flanks of the magnetotail. As pointed out by Dandouras, such a model avoids the non-physical features introduced by a sharp bend in the neutral sheet at $Y_{AGSM}=Y_0$ in the single ellipse neutral sheet models used by *Fairfield* [1980] and in this study. Fortunately, the locus of the bend occurs at the boundary in the present work. We found that the maximum east-west extent of the magnetopause is 20.4 $R_E$ while $Y_0$ was found to be 20.2 $R_E$, and thus there is no sharp bend in the model presented here for any of the dipole tilt bins.

The analytic model of *Voigt* [1984] predicts a neutral sheet that decreases in curvature as distance down the tail increases due to the reduced influence of the tilted dipole at large distances. Figure 7 from Figure 4 of *Voigt* [1984] shows current streamlines for downtail distances of 15 and 30 $R_E$ and a dipole tilt of 35°. The middle streamline in each case represents the neutral sheet. The neutral sheet crosses the $XY$ plane at approximately 9 $R_E$ for $X_{AGSM}$=-15 $R_E$ and 14.5 $R_E$ for $X_{AGSM}$=-30 $R_E$. The model of Voigt assumes a cylindrical magnetopause with a fixed radius of 20 $R_E$ and thus the change in curvature of the neutral sheet in Figure 7 is due solely to the reduced influence of the tilted dipole at large distance. The observations presented in this study also have the effect of tail flaring removed and thus can be compared directly to the model of Voigt. Plate 4 shows cross sectional images of the neutral sheet for down tail distances of -15 ≥ $X_{AGSM}$ > -25 and -25 ≥ $X_{AGSM}$ > -35. Asterisks mark the point where the Voigt neutral sheet crosses the $XY$ plane. We have scaled this distance by the ratio 21.2/20.0, the ratio of the approximate magnetopause radius of this study to the 20 $R_E$ radius used by Voigt. While the lack of data in Plate 4 prevents a neutral sheet model from being determined separately for the two downtail distance bins, it is clear that the large change in neutral sheet curvature in the model of Voigt is not seen. This result agrees with the result of *Fairfield* [1980] that the downtail distance effect on neutral sheet curvature is small. It should be stressed that the observations in the range -25 $R_E$ < X < -15 $R_E$ in Plate 4 are taken throughout this range of $X$ distances whereas the Voigt model was evaluated for X=-15 $R_E$ .

We have mentioned above that the *Dandouras* [1988] model is based on ISEE data taken closer to the earth than the IMP data set used by *Fairfield* [1980]. The sparseness of the present data set once decimated by the restriction in downtail distance is obvious in Plate 4. We are not able to generate neutral sheet models separately for the two dipole tilt bins. It is possible that the neutral sheet is of the form given by the Dandouras model in the near tail and changes to the elliptical shape of Fairfield farther downtail. However, this would require a process that changes the neutral sheet alignment near the flanks from one parallel to the $XY$ plane to a continuously curved shape as downtail distance increases. As we have not identified a reasonable mechanism, we believe the difference in the two shapes should be attributed to the functional form of the neutral sheet model selected by Dandouras. We avoid the need to choose a functional form a priori by first creating the image of the neutral sheet and then picking a model that is suggested by the data. However, we cannot completely rule out the possibility that our results do not apply closer to Earth.

Recently, *Ohtani and Kokubun* [1990] presented a model magnetopause with a rather severe flattening in the north-south direction. Their magnetopause model has a semimajor axis (parallel to $Y_{AGSM}$) of 27 $R_E$ and a semiminor axis (parallel to $Z_{AGSM}$) of only 23 $R_E$. Ohtani and Kokubun noted that this result should be treated with caution. The magnetopause boundaries shown in Figure 4 are in direct conflict with the model of Ohtani and Kokubun. In light of the warnings given by Ohtani and Kokubun, their lack of any magnetopause crossings at low latitudes, and the large spread in radial distance of their magnetopause crossings, one is safe in saying that the strongly elliptical average magnetopause shape suggested by Ohtani and Kokubun is not a realistic description of the tail boundary.

MHD simulations by *Walker et al.* [1989] show a distortion of the magnetopause with dipole tilt with the magnetopause becoming egg shaped for large dipole tilts. The magnetopause in the simulation looks slightly top heavy with the east west extent of the northern lobe slightly larger than the southern lobe during intervals of large positive dipole tilts. Such a shape could be modeled by the introduction of a cubic term in $Z_{AGSM}$ under the radical of (3) and would provide an acceptable fit to the magnetopause seen in Plate 2*b*. However, the lack of data at high latitudes in the northern hemisphere means this cubic term would not be well constrained. In Plate 2 any contraction of the southern lobe due to the "eggness" of the magnetopause would be indistinguishable from the effect of the displacement of the magnetopause. Because of the lack of data at high northern latitudes to constrain the fit, we have selected a model with fewer parameters, i.e., (3).

Figure 4 and Plate 2 show that the magnetopause boundary contracts along the southern lobe as the dipole tilt angle increases. This contraction appears to be the result of the displacement of the magnetopause along the $Z_{AGSM}$ axis. The displacement of the magnetopause along the $Z_{AGSM}$ axis is necessary to balance the average magnetic flux by requiring equal areas in the lobes assuming equal field magnitudes in the lobes. Figure 8 shows that the value $Bx_{North\ Lobe}+Bx_{South\ Lobe}$ for the 5° bins of dipole tilt is small and thus demonstrates that the assumption of equal average field magnitudes in the two

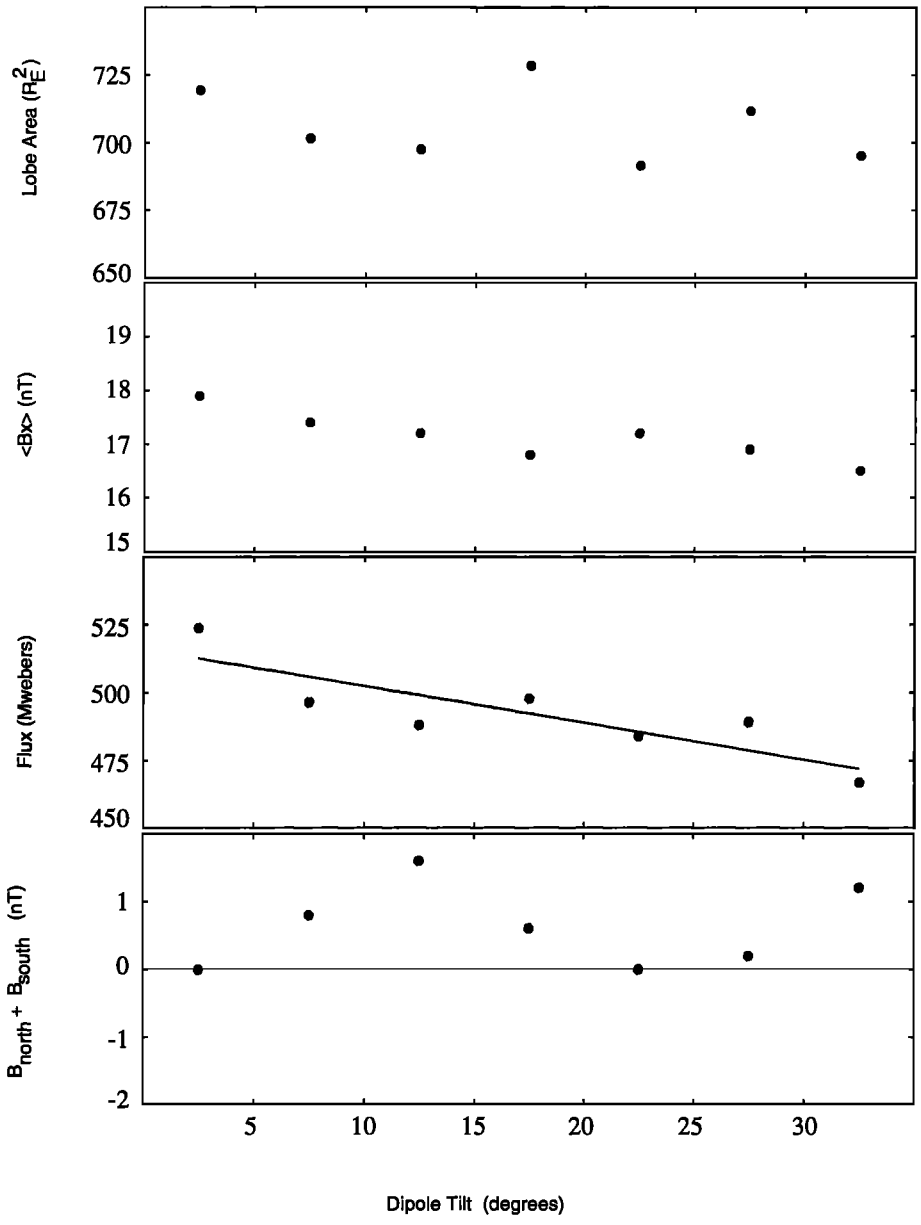


Fig. 8. Lobe area, average $B_x$ in the lobes, magnetic flux (line gives a least squares fit), and the difference between the observed value of $|B_x|$ in the northern and southern lobes.

lobes is well satisfied. In each dipole tilt bin the difference between $B_x$ in the northern and southern lobe is less than 2 nT. With this condition on $B_x$, to maintain equal flux in the lobes requires equal lobe areas. The displacement of the magnetopause seen in Figure 4 and Plate 2 would appear to be the response of the magnetopause required to satisfy the condition of equal lobe flux.

Figure 8 shows that the area of the tail is approximately constant while $B_x$ decreases with increasing dipole tilt. The standard deviation of $B_x$ measured in the lobes in this study is typically 5 nT, and therefore the trend seen in $B_x$ in Figure 8 is within the ±1 standard deviation, but it is not clear that the standard deviation gives an accurate representation of the error in the measurements. Bins near the plasma sheet or magnetosheath will contain some data from the magnetosheath or plasma sheet. In these bins close to the plasma sheet or sheath the medians are skewed accounting for the rather large standard deviations. Our failure to account for the solar wind dynamic pressure effect on the field magnitude probably also produces a broad distribution of lobe field magnitudes. However, the fact that in completely independent measurements the northern and southern lobe field magnitudes agree to within less than 2 nT (out of 17 nT) suggests that the actual error in $B_x$ is well within the limits given by the standard deviation and that the trend is significant. A decrease in magnetic flux in the tail lobe with increasing dipole tilt could be related to the seasonal variation in activity [*Chapman and Bartels*, 1940]. *Russell and McPherron* [1973] have accounted for seasonal variations of activity by noting that the orientation of the dipole favors reconnection with the solar wind magnetic field for field orientations typical of March and September, times of small dipole tilt. Thus increased lobe flux for small dipole tilt may result from the increased probability of adding open flux to the tail. *Kivelson and Hughes* [1990]

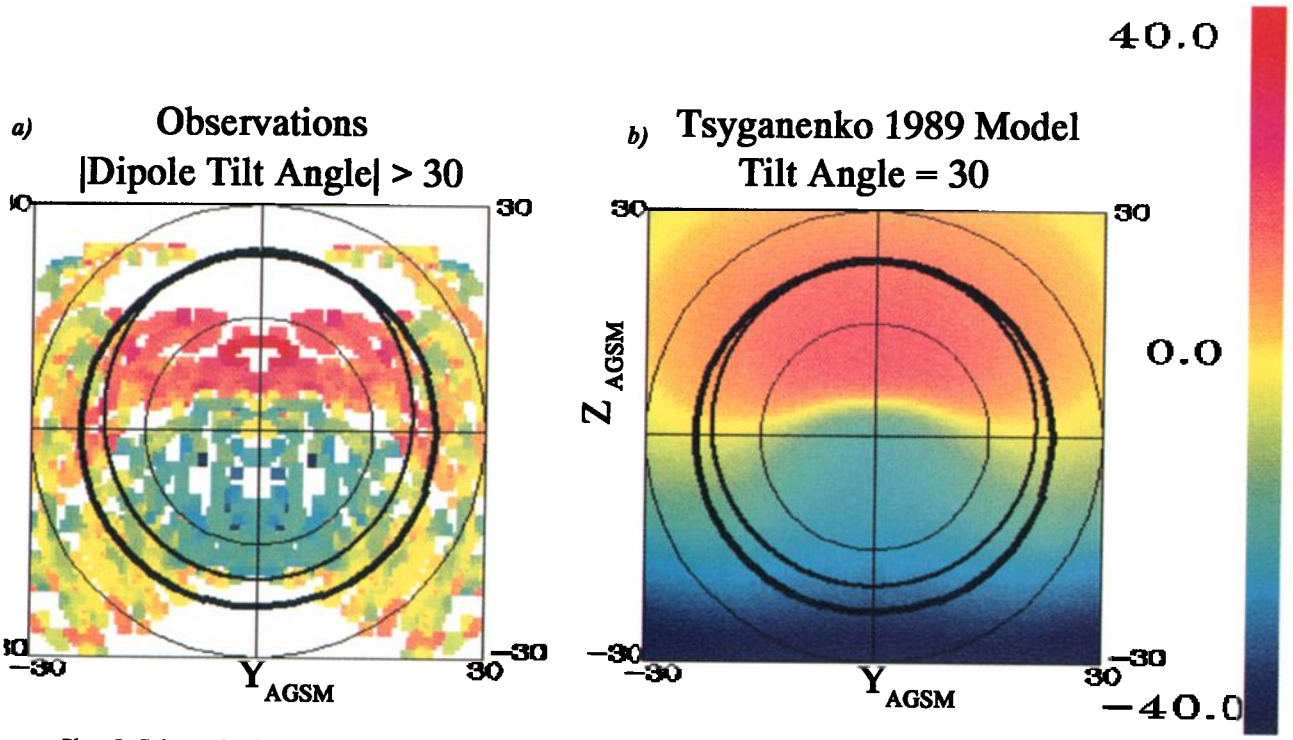


Plate 5. Color scale gives $B_x$ in nanoteslas for $60 \times 60$ $R_E$ cross sections of the magnetotail at $X_{AGSM}$=-25 $R_E$ *(a)* median $B_x$ observed during times when the absolute value of the dipole tilt angle was > 30° for a nominal solar wind dynamic pressure of 3.8 nPa. *(b)* Value of $B_x$ from the Tsyganenko 1989 model for a dipole tilt of 30° and $Kp$=2.

have suggested that small substorms occur more frequently during times of high dipole tilt. If this is true, then the lobe flux would be reduced by frequent small substorms. Our data set does not enable us to assess the relative contributions of these two mechanisms.

The images of the cross section of the average magnetotail presented here give a picture of the magnetotail structure. Global magnetospheric models such as the Tsyganenko 1989 model [*Tsyganenko*, 1989] are empirical fits to averaged data. The advantage of imposing functions to describe the average magnetic structure is that functions allow evaluation at any spatial point, and thus the Tsyganenko model is more tractable than images. Unlike images, models such as the Tsyganenko model must impose a form of the currents and neutral sheet. Conclusions drawn from these models are dependent on assumptions about fitting curves and the location of currents. Plates 5 and 6 compare the images presented here with the Tsyganenko 1989 model for 30° and 0° dipole tilts respectively. In evaluating the Tsyganenko model in Plates 5 and 6 a $Kp$ value of 2 was used. A downtail distance of -25 $R_E$ was used to be consistent with the -25 $R_E$ reference distance used in the present work. The magnitude of the observed and model fields agree fairly well. In contrast, during periods of large dipole tilt, the two neutral sheets differ, with the Tsyganenko model underestimating the curvature of the neutral sheet near the flanks. In Plate 6 the effects of tail flaring and the closure of the field through the plasma sheet is clear in both the Tsyganenko model and the images. It is evident that the functions producing $B_y$ and $B_z$ in the Tsyganenko model have very sharp boundaries compared to the more diffuse transition regions in the images presented in this study.

## CONCLUSIONS

We have created an image of a cross-sectional slice of the magnetotail for a range of dipole tilt angles. Evident in these images are the magnetospheric boundaries which define the magnetotail: the magnetopause and the neutral sheet. The primary advantage of an imaging-based technique in observing magnetotail boundaries is that the shape of the boundaries is determined directly from the images. In addition, as a refinement to previous studies we have scaled spatial coordinates by solar wind dynamic pressure and have accounted for the effects of tail flaring on both the field and spatial coordinates.

Near the flanks of the magnetotail, the neutral sheet image is close to the Fairfield model [*Fairfield*, 1980] but curves slightly more than that model. During times of large dipole tilt angle, the neutral sheet appears to have the basic displaced elliptical shape suggested by Fairfield rather than flattening out near the flanks as suggested by the analytic model of *Voigt* [1984] and fits of *Dandouras* [1988]. The sharp (and unphysical) bend in the model neutral sheet of *Fairfield* [1980] occurring at $Y_{AGSM}=Y_0$ is not encountered in the present model because the east-west extent of the magnetopause is approximately equal to $Y_0$. During times of large dipole tilt angle the Tsyganenko 1989 model underestimates the curvature of the neutral sheet. This is consistent with the good agreement between the neutral sheet models of Tsyganenko and Dandouras [*Tsyganenko*, 1990]. The large decrease in curvature of the neutral sheet with increasing downtail distance seen in the analytic magnetospheric model of *Voigt* [1984] is not observed in the magnetotail images presented here.

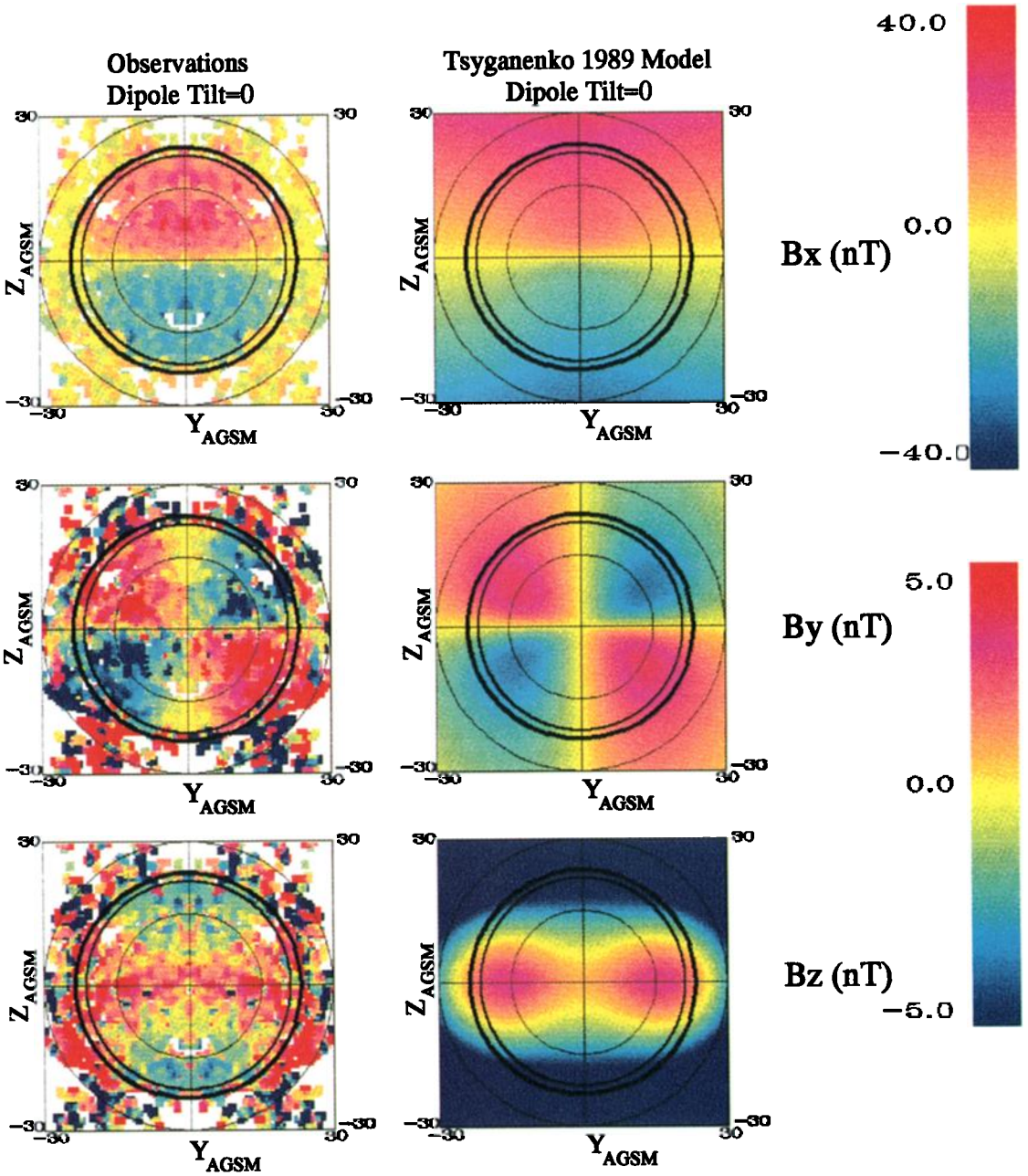


Plate 6. Color scale gives $B_x$ (from -40 to 40 nT) and $B_y$ and $B_z$ (from -5 to 5 nT) for 60 × 60 $R_E$ cross sections of the magnetotail at $X_{AGSM}$=-25 $R_E$. Left-hand panels display the median $B_x$, $B_y$, and $B_z$ observed during times when the absolute value of the dipole tilt angle was < 5° for a nominal solar wind dynamic pressure of 3.8 nPa. Right-hand panels display $B_x$, $B_y$, and $B_z$ from the Tsyganenko 1989 model for a dipole tilt of 0° and $Kp$=2.

It appears that three independent determinations of the form of the tail neutral sheet [*Voigt*, 1984; *Dandouras*, 1988; and *Tsyganenko*, 1989] disagree with the neutral sheet model presented here. However, as we have seen, Dandouras based his work on the analytic model of Voigt. Thus the two models are not independent of one another. The Voigt model provides a useful analytic model of the magnetosphere but because of its analytic form it has certain limitations. We have shown that the strong downtail distance effect on neutral sheet curvature present in the Voigt model is not observed in our data. In addition, Voigt's assumptions of a nonflaring circular magnetopause adopted to provide a tractable analytic solution is not observed. It is understandable, then, that an empirical model based on a simplified analytical model differs near the boundary from the model developed in this study. The Tsyganenko model is a global semiempirical model that is not optimized to model the neutral sheet specifically.

Our model implies that when the dipole is tilted, some of the currents flowing from the neutral sheet must bend through an angle greater than 90° before flowing around the lobe. A very abrupt rotation of current is evidently unphysical whether in our model or in the Dandouras model where currents abruptly

bend through 90° at the magnetopause. In the real magnetosphere the plasma sheet becomes thicker near the flanks. This implies that the currents become more diffuse as they turn to flow around the lobes. Possibly the observed thickening of the plasma sheet near the flanks is required for this precise reason.

The magnetopause appears to be slightly elliptical with a semimajor axis in the north-south direction of 22 $R_E$ and a semiminor axis in the east-west direction of 20.4 $R_E$ giving an eccentricity of ~0.37. These values do not appear to vary appreciable with dipole tilt angle. The center of the ellipse moves along the $Z_{AGSM}$ axis with increasing dipole tilt. The suggestion of *Ohtani and Kokubun* [1990] that the time-averaged magnetopause boundary is severely flattened in the north south direction is not supported by the present work. Close to the Earth, *Sibeck et al.* [1991] have shown that the magnetopause is flattened in the north-south direction by 8%. It is interesting to note that in the range $-15\ R_E < X < -5\ R_E$, Sibeck et al. find a magnetopause elongated in the north-south direction. However, Sibeck et al. caution that the error at these distances in their study is large.

For a given dipole tilt the assumption of equal field magnitudes on average in the northern and southern lobes appears to be well satisfied. With increasing dipole tilt the field magnitude decreases and thus the total flux in each lobe is on average smaller during times of large dipole tilt angle. If real, this result would be consistent with the seasonal variation in geomagnetic activity, with less reconnected flux being present in the tail on average during the winter and summer solstices.

*Acknowledgments.* The authors wish to thank N. Ness, R. Lepping, and the NSSDC for supplying the IMP 7 and IMP 8 magnetometer data and C. Russell for providing the ISEE 2 magnetometer data. This work was supported by NASA grants NGT 50618 and NAG5-1529.

The Editor thanks D. Fairfield and J. S. Dandouras for their assistance in evaluating this paper.

## REFERENCES

Behannon, K. W., Mapping of the Earth's bow shock and magnetic tail by Explorer 33, *J. Geophys. Res.*, *73*, 907, 1968.

Bowling, S. B., The influence of the direction of the geomagnetic dipole on the position of the neutral sheet, *J. Geophys. Res.*, *79*, 5155, 1974.

Bowling, S. B., and C. T. Russell, The position and shape of the neutral sheet at 30-$R_E$ distance, *J. Geophys. Res.*, *81*, 270, 1976.

Chapman, S., and J. Bartels, *Geomagnetism*, chap. 11, Oxford University Press, New York, 1940.

Couzens, D. A., and J. H. King, *Interplanetary Medium Data Book-Supplement 3, 1977--1985*, National Space Science Data Center, Washington, D. C., 1986.

Dandouras, J., On the average shape and position of the geomagnetic neutral sheet and its influence on plasma sheet statistical studies, *J. Geophys. Res.*, *93*, 7345, 1988.

Fairfield, D. H., and N. F. Ness, Configuration of the geomagnetic tail during substorms, *J. Geophys. Res.*, *75*, 7032, 1970.

Fairfield, D. H., A statistical determination of the shape and position of the geomagnetic neutral sheet, *J. Geophys. Res.*, *85*, 775, 1980.

Gosling, J. T., D. J. McComas, M. F. Thomsen, S. J. Bame, and C. T. Russell, The warped neutral sheet and plasma sheet in the near-Earth geomagnetic tail, *J. Geophys. Res.*, *91*, 7093, 1986.

Howe, H. C., Jr., and J. H. Binsack, Explorer 33 and 35 plasma observations of the magnetosheath flow, *J. Geophys. Res.*, *77*, 3334, 1972.

Kivelson, M. G., and W. J. Hughes, On the threshold for triggering substorms, *Planet. Space Sci.*, *38*, 221, 1990.

Mihalov, J. D., D. S. Colburn, R. G. Currie, and C. P. Sonett, Configuration and reconnection of the geomagnetic tail, *J. Geophys. Res.*, *73*, 943, 1968.

Murayama, T., Spatial distribution of energetic electrons in the geomagnetic tail, *J. Geophys. Res.*, *71*, 5547, 1966.

Nakai, H., Y. Kamide, and C. T. Russell, Influences of solar wind parameters and geomagnetic activity on the tail lobe magnetic field: A statistical study, *J. Geophys. Res.*, *96*, 5511, 1991.

Ohtani, S., and S. Kokubun, Imp 8 magnetic observations of the high latitude tail boundary: locations and force balance, *J. Geophys. Res.*, *95*, 20759, 1990.

Peredo, M., and D. P. Stern, On the position of the near-Earth neutral sheet: A comparison of magnetic model predictions with empirical formulas, *J. Geophys. Res.*, *96*, 19521, 1991.

Petrinec, S. P., P. Song, and C. T. Russell, Solar cycle variations in the size and shape of the magnetopause, *J. Geophys. Res.*, *96*, 7893, 1991.

Russell, C. T., and K. I. Brody, Some remarks on the position and shape of the neutral sheet, *J. Geophys. Res.*, *72*, 6104, 1967.

Russell, C. T., and R. L. McPherron, Semiannual variation of geomagnetic activity, *J. Geophys. Res.*, *78*, 92, 1973.

Russell, C. T., and S. M. Petrinec, On the relative intercalibration of solar wind instruments on IMP-8 and ISEE-3, *Geophys. Res. Lett.*, *19*, 961, 1992.

Sibeck, D. G., R. E. Lopez, and E. C. Roelof, Solar wind control of the magnetopause shape, location, and motion, *J. Geophys. Res.*, *96*, 5489, 1991.

Tsyganenko, N. A., A magnetospheric magnetic field model with a warped tail current sheet, *Planet. Space Sci.*, *37*, 5, 1989.

Tsyganenko, N. A., Quantitative models of the magnetospheric magnetic field: methods and results, *Space Sci. Rev.*, *54*, 75, 1990.

Voigt, G-H., The shape and position of the plasma sheet in Earth's magnetotail, *J. Geophys. Res.*, *89*, 2169, 1984.

Walker, R. J., T. Ogino, and M. Ashour-Abdalla, Simulating the magnetosphere: The structure of the magnetotail, in *Solar System Plasma Physics, Geophys. Monogr. Ser.*, vol. 54, edited by J. H. Waite, Jr., J. L Burch, and R. L. Moore, p. 61, AGU, Washington, D. C., 1989.

C. M. Hammond, Los Alamos National Laboratory, Mail Stop D466, Los Alamos, NM 87545.

M. G. Kivelson and R. J. Walker, Institute of Geophysics and Planetary Physics, University of California, Los Angeles, CA 90024.

(Received August 31, 1992; revised April 27, 1993; accepted June 25, 1993.)